Springer

KSME

Journal of Mechanical Science and Technology 24 (2010) 639~648
www.springerlink.com/content/1738-494x
DOI 10.1007/s12206-010-0110-4

Prediction of flow stress of metallic material and interfacial friction condition at high temperature using inverse analysis†

Kyungmin Shin, Sukhwan Chi and Naksoo Kim*

Depatment of Mechanical Engineering, Sogang University, Seoul, 121-742, Korea

(Manuscript Received December 31, 2007; Revised September 16, 2009; Accepted December 8, 2009)

Abstract

Inverse analysis is a method for determining material parameters by minimizing the difference between experimental and the finite element (FE) simulated results, such as the load-stroke curve and barreling shape of a deformed specimen using an optimum design technique. In this study, ring compression tests were conducted to predict the flow stress of materials and interfacial friction conditions. Cylinder compression tests were conducted under the same process conditions to estimate the validity of the data obtained from the ring compression tests. By comparing the experimental results with the FE simulated results, it was confirmed that flow stress and the interfacial friction condition obtained from the ring compression tests, as well as their inverse analysis, are quite reasonable. The validity of both the flow stress function and the interfacial friction condition using the above procedures was verified by the experiments.

Keywords: Flow stress function; Inverse analysis; Finite element (FE) simulation; Interfacial friction condition

1. Introduction

Rheological features, such as the flow stress of a material and the friction conditions in metal forming processes, are important issues that must be considered during the design process; they affect the forming characteristics of materials. Recently, the finite element (FE) simulation of a metal forming process has enabled reductions in the cost and time by predicting the results of real forming processes. The accuracy of the FE simulated results depends on the precision of the information, such as the flow stress of the materials and the interfacial friction condition. However, it is still difficult to accurately express them in hot working conditions. When predicting the results of real processes through the FE simulation, it is important to determine the above parameters.

Nowadays, a new method called inverse analysis has been proposed for determining the material properties. The general concept of this method is based on a combination of the FE simulation of selected material tests and the experimental measurement of the parameters, such as the force or torque.

In this paper, inverse analysis was applied to determine the flow stress of materials and the interfacial friction condition in hot forming processes. Many researchers had performed studies using inverse analysis, which minimizes the difference between the experimental and the FE simulated results in determining the flow stress of materials and the friction condition [1-5]. In order to evaluate the friction conditions precisely, many researchers conducted studies about the barreling shape of a deformed specimen in a cylinder compression test. The friction conditions could be determined by applying an upper bound method including unknown coefficients to the cylinder compression test [6-8]. In order to better understand the characteristics of the friction conditions, a geometrical model of the barreling shape of the deformed specimen was developed, and its validity was verified by comparing it with the experimental results [9-16].

In this paper, on the basis of the reliability of inverse analysis, the unknown coefficients of a new flow stress function proposed by Kim and Choi [17] and the interfacial friction conditions were determined. They were verified by ring and cylinder compression experiments.

2. Theoretical background

2.1 Flow stress function

Several researchers have attempted to mathematically express the flow stress of a material in hot working conditions [18-22]. However, they required the microstructural information of the materials. Therefore, these methods are not efficient since complicated and many experiments were conducted to obtain the

† This paper was recommended for publication in revised form by Associate Editor Youngseog Lee

*Corresponding author. Tel.: +82 2 705 8635, Fax.: +82 2 712 0799
E-mail address: nskim@sogang.ac.kr

microstructural information of materials.

On the other hand, the flow stress function proposed by Kim and Choi [17] can describe metal flows accompanied with phenomena such as dynamic recrystallization and recovery at high temperatures without microstructural access. This flow stress function includes the modified Zener-Hollomon (Z') parameter, which adds unknown coefficients to the temperature and strain-rate terms of the existing Zener-Hollomon (Z) parameter to increase its temperature and strain-rate sensitive.

This paper used the above flow stress function and it is defined as follows:

$$\sigma_f = \left(a_0 + \frac{a_1}{T}\right)\bar{\varepsilon}^n U^m \left\{1 + \exp\left[-a_2 \frac{\bar{\varepsilon} - \varepsilon_p}{\varepsilon_b}\right] - \exp\left[-a3\frac{\bar{\varepsilon}}{\varepsilon_b}\right]\right\}, \quad (1)$$

$$\begin{cases} \varepsilon_p = a_4 U + a_5 \\ \varepsilon_p = a_6 U + a_7 \\ U = \ln(Z') \\ Z' = k\dot{\bar{\varepsilon}}^p \exp\left[\dfrac{Q_{def}}{RT}\right] \end{cases}, \quad (2)$$

where $\bar{\varepsilon}$ is the effective strain, $\dot{\bar{\varepsilon}}$ is the effective strain rate, Z' is the modified Zener-Hollomon parameter, T is the temperature in K, R is the gas constant, and n, m, k, p, and a_0–a_7 are the unknown coefficients determined by inverse analysis. The apparent activation energy Q_{def} for hot deformation in Z' was calculated from the measurements of loads using a simplified graphical method, described in Ref. 23. The activation energy Q_{def} of materials was different. However, 483000 kJ/mol, the known average value, was used instead.

3. Methodology

3.1 Inverse analysis algorithm

The 12 unknown coefficients in Eqs. (1) and (2) were determined by minimizing the difference in the load-stroke data between the experimental and FE simulated results using inverse analysis. The numerical method used in the inverse analysis is an optimum technique.

In order to apply the inverse analysis, the design parameters and the object function must be established preferentially. The flow stress of the materials and the interfacial friction condition were predicted by the axisymmetric ring compression tests. The object function that was minimized has the following form:

$$\Phi(x_1, x_2, \cdots, x_k) = \sqrt{\frac{1}{n}\sum_{i=1}^{n}\left(\frac{F_i^c - F_i^m}{F_i^m}\right)^2}, \quad (3)$$

where x_1, x_2, ..., x_k are the rheological parameters, n is the total number of sampling points in the measurements, the subscript i is the number of measurements, and F_i^m and F_i^c are the measured and calculated loads at a given i, respectively.

3.2 Procedure for flow stress function determination

In this study, the object function in Eq. (4) was modified in order to reflect the effect of the compression velocity affecting the deformation behavior of the material in Eq. (3) [24]. Compression tests were conducted with two different compression velocities for each temperature, and isothermal condition was assumed during compression. In other words, after conducting the compression tests with two different velocities V_1 and V_2 at the same temperature, the difference between two load-stroke data obtained from tests and the results of FE analysis were minimized simultaneously,

$$\Phi(x_1, x_2, \cdots, x_k) = \sqrt{\frac{1}{2}\sum_{i=1}^{2}\left[\frac{1}{Ns}\sum_{j=1}^{Ns}\left(\frac{F_{ij}^c - F_{ij}^m}{F_{ij}^m}\right)^2\right]}\Bigg|_r, \quad (4)$$

where F_{ij}^m and F_{ij}^c are the measured and calculated loads, respectively. Ns is the number of sampling points. By minimizing the above object function, the unknown coefficients in the flow stress function were determined. The gradient method including the golden section search and conjugate gradient method were considered for minimizing the object function [25]. Its convergence criteria were indicated if

$$\left\|\frac{\partial \Phi_1}{\partial x_k}\right\| < \varepsilon_1, \quad (5)$$

$$\left|\frac{x_k^{(s+1)} - x_k^{(s)}}{x_k^{(s)}}\right| < \varepsilon_2, \quad (6)$$

where s is an iteration number and ε_1 and ε_2 are the specified tolerances, both 0.001.

3.3 Procedure for interfacial friction condition determination

The interfacial friction is one of dissipation of energy that it generates heat and the accompanied rising of temperature could have serious influence on the overall forming process. Since free behaviors of the contact surfaces are interrupted by the friction, the friction has an effect on the deformation behavior of the material and a forming load in the metal forming process. Therefore, the interfacial friction should be considered in order to determine the precise flow stress.

In this paper, the friction factor (m_f) was used as the factor describing the interfacial friction condition. The ring compression test is one of the methods measuring the friction factor and is especially used in the plastic forming process. This test determined the interfacial friction condition by measuring the barreling of the material after compressing the ring specimen. In order to determine the friction conditions, the inverse analysis was employed. After extracting and discretizing the outer shape of the barreling of the compressed specimen, the friction was determined by minimizing the difference between the extracted shapes from the experiment and simulation re-

sults. The reason for using only the outer shape of the barreling is the difficulty in measuring the inner shape of the barreling. In applying the inverse analysis, the variable is the friction factor and the object function is minimized and has the following form:

$$\Phi_2\left(m_f\right)=\left|\frac{A_m^{OR}-A_c^{OR}}{A_m^{OR}}\right|, \tag{7}$$

where A_m^{OR} and A_c^{OR} refer to the area enclosed by the measured and calculated outer radius, respectively. The friction factor was determined by using the optimization technique, which is equal to the method used in minimizing Eq. (4). Its convergence criteria were indicated if

$$\left\|\frac{\partial\Phi_2}{\partial m_f}\right\|<\varepsilon_3, \tag{8}$$

$$\left|\frac{m_f^{(s+1)}-m_f^{(s)}}{m_f^{(s)}}\right|<\varepsilon_4, \tag{9}$$

where s is an iteration number and ε_3 and ε_4 are the specified tolerances, both 0.001.

Digital image processing techniques (Sobel edge- detection algorithm) were used for extracting the barreling shape of the specimen [26]. The coordinates of the extracted image were plotted using the cubic-spline curves of the measured and calculated outer barreling shapes.

3.4 Total algorithm for inverse analysis

Fig. 1 shows the total algorithm of the inverse analysis. As the friction factor is an arbitrary constant, the unknown coeffi cients of the flow stress function were determined by minimizing the difference of load-stroke data between experimental and FE simulation results. After the determined coefficients of flow stress function were fixed, the friction factor was determined by minimizing the difference in the areas enclosed by two cubic-spline curves of the measured and calculated outer barreling shapes. Since the load-stroke data were changed with changing the friction factor, the flow stress should be determined again. Then, the unknown coefficients of the flow stress function determined from the previous iteration were used as the initial values of the coefficients of the flow stress function in the present iteration. The computing time decreased definitely as compared with the previous iteration because the change in the load data by the friction factor was not large. By repeating the above process, the flow stress and the interfacial friction condition, which minimized the difference in load-stroke data and the shape of barreling between the experiment and the FE simulation results, can be determined simultaneously.

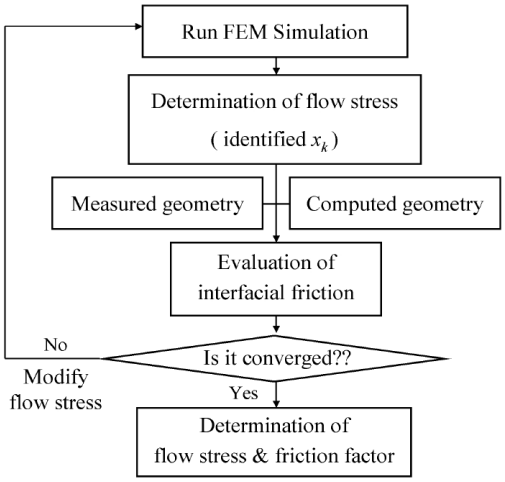

Fig. 1. Flow chart of the determination of the flow stress and the friction factor by inverse analysis.

4. Experiment setup and conditions

4.1 Specification of the work piece and compression machine

In the experiment, the size of the used ring specimens is shown in Fig. 2, and the compression rate was 50%. In order to verify the flow stress and the interfacial friction conditions drawn by the ring compression tests, cylinder compression tests were conducted using the same materials. The size of the cylinder specimens is shown in Fig. 3. The equipment used in the compression test at high temperatures was SGA-GP1000 (Fig. 4), which can be heated up to 1400° C and whose maximum load is 1000 kN.

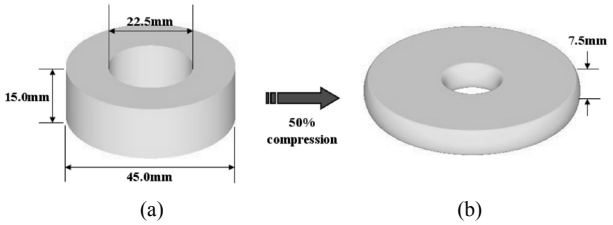

Fig. 2. Size of the ring specimen: (a) before compression and (b) after compression.

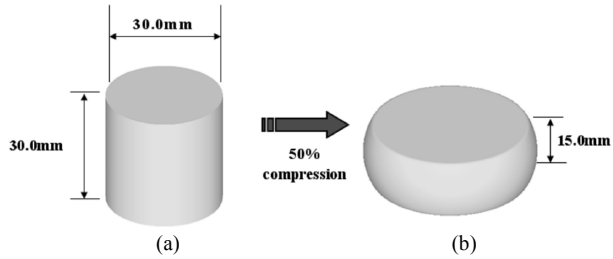

Fig. 3. Size of the cylinder specimen: (a) before compression and (b) after compression.

Table 1. Experimental conditions.

	Temperature (℃)	Compression velocity (mm/sec)	
		V_1	V_2
Material A	900	0.2	0.8
	950		
Material B	950	0.2	0.8
	1000		

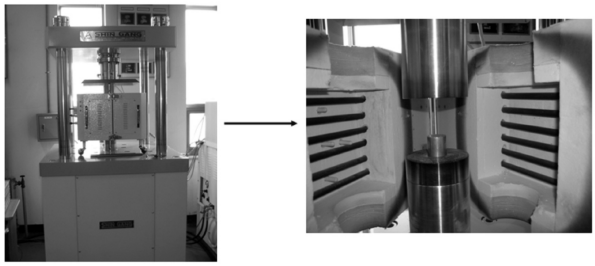

Fig. 4. Experimental equipment (SGA-1000, compression machine).

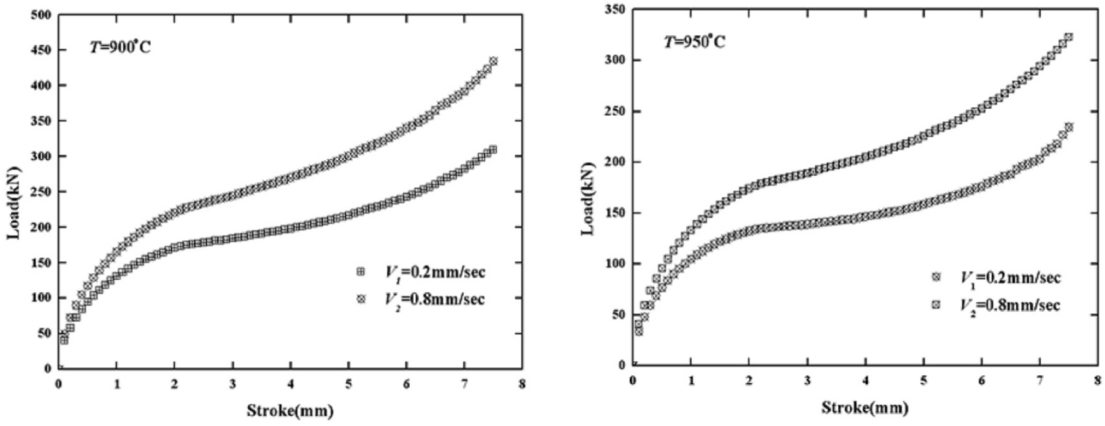

(a) (b)

Fig. 5. Load-stroke curve obtained from experiments (Material A): (a) 900℃ and (b) 950℃.

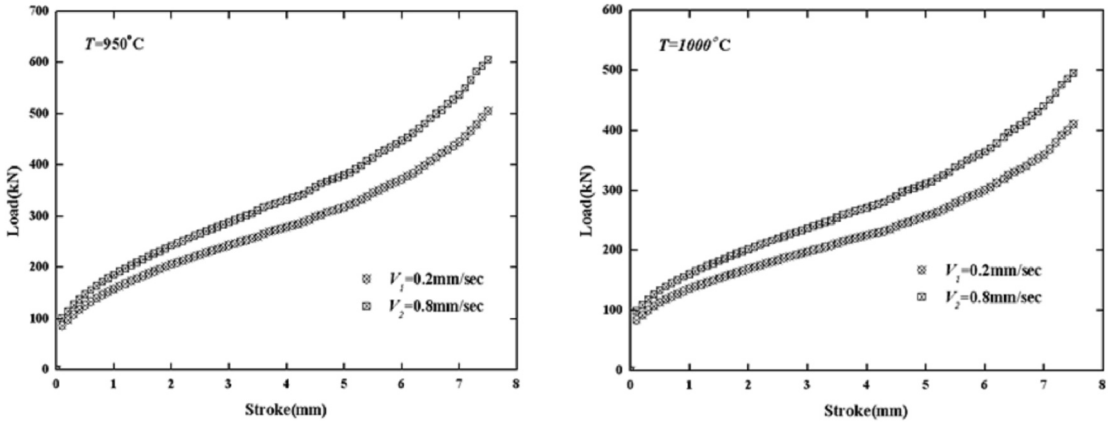

(a) (b)

Fig. 6. Load-stroke curve obtained from experiments (Material B): (a) 950℃ and (b) 1000℃.

4.2 Experimental conditions

Two types of materials were used in the experiment. The purpose of this study was to determine the material properties that are acquired to predict the results of the real forming process by using the FE simulation. Assuming that information about the materials does not exist, the materials were designated as material A and Material B. In addition, two materials were not operated with the same temperature by FE simulation and experiment. Hence, these conditions depict a more general situation. The experimental conditions for each material are listed in Table 1.

5. Results and discussion

5.1 Determination of flow stress and interfacial friction condition

Using the experimental conditions described above, the commercially available FEM code DEFORM 2D v8.2 was used as the FE simulation program, which was used to minimize the object function based on the load-stroke data. Figs. 5 and 6 show the load-stroke graph drawn by the ring compres-

sion tests. Figs. 7 and 8 show that the difference in the load-stroke curves between the experiments and FE simulations was decreased through inverse analysis. Finally, the computed and experimental loads were nearly identical, as shown in Figs. 7 and 8. The above results suggest the flow stress function determined by inverse analysis can suitably express the rheological phenomenon of each material.

When minimizing the object function, the selection of the

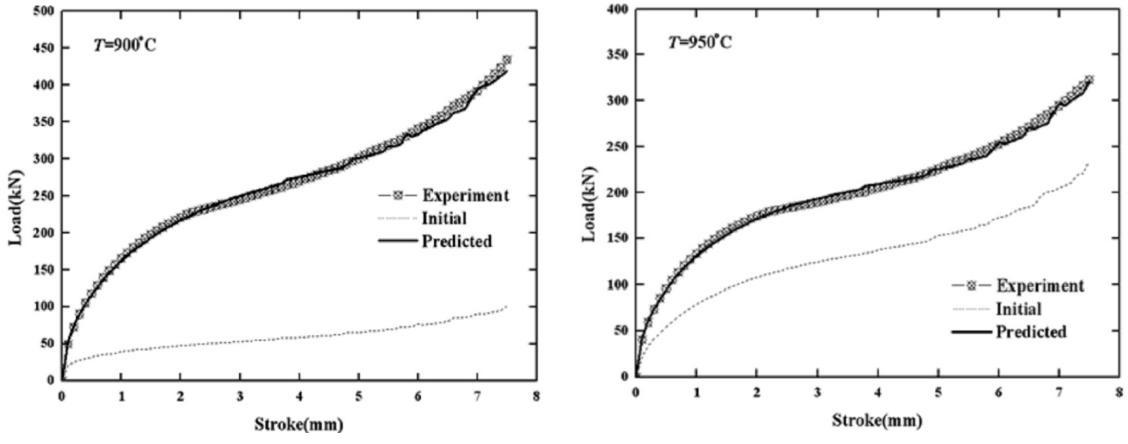

(a) (b)

Fig. 7. Compression of the experimental load-stroke curve and computed curve with V=0.8mm/s (Material A): (a) 900℃ and (b) 950℃.

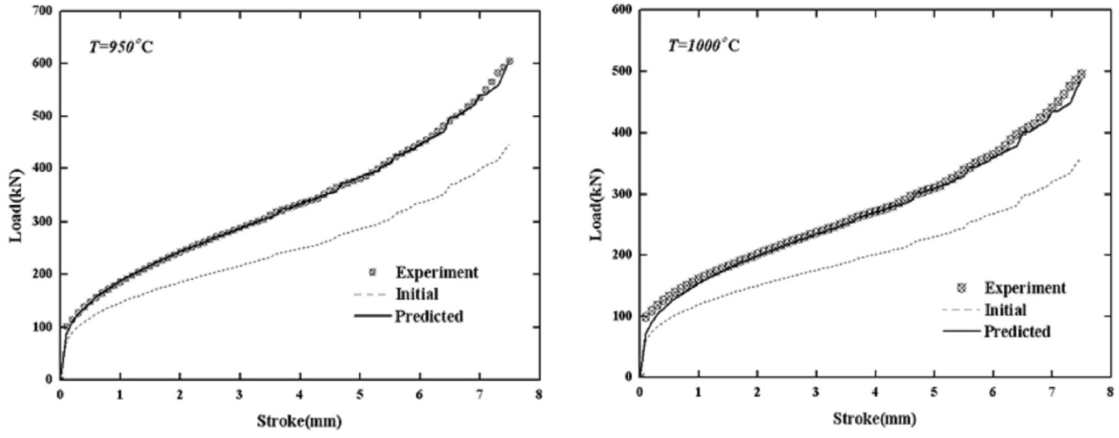

(a) (b)

Fig. 8. Compression of the experimental load-stroke curve and computed curve with *V*=0.8mm/s (Material B): (a) 950℃ and (b) 1000℃.

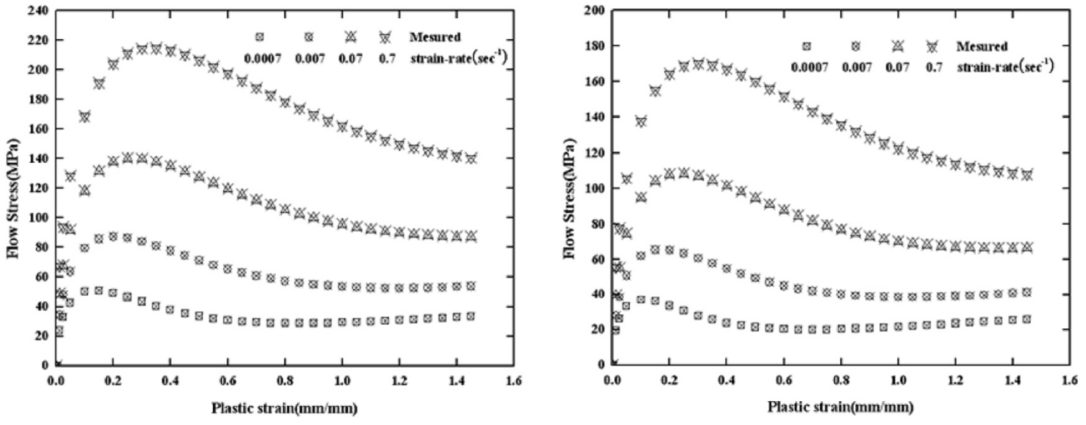

(a) (b)

Fig. 9. Stress-strain curve obtained from inverse analysis for Eq. (1) and (2). (Material A): (a) 900℃ and (b) 950℃.

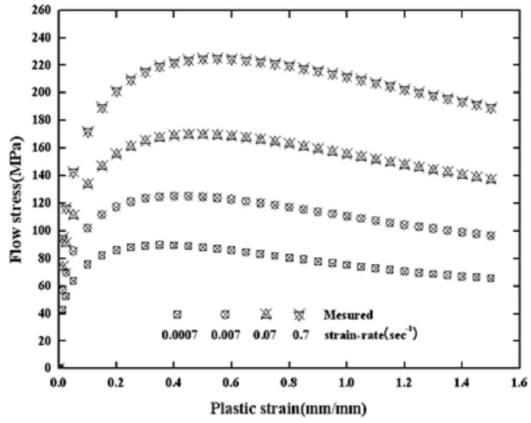

(a)

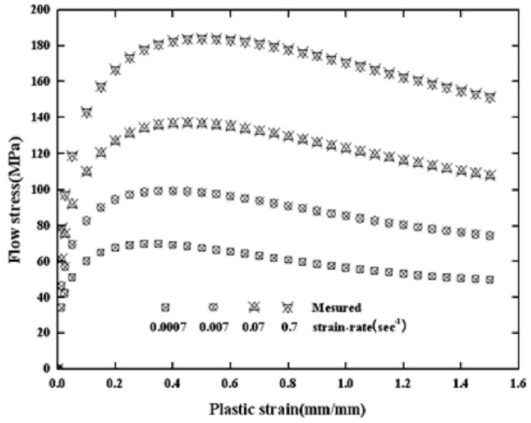

(b)

Fig. 10. Stress-strain curve obtained from inverse analysis for Eq. (1) and (2). (Material B): (a) 950℃ and (b) 1000℃.

initial value of the unknown coefficients is of importance. In particular, an unsuitable initial value may yield a result that interferes with the convergence because the object function given in Eq. (4) is nonlinear. Therefore, in order to minimize the object function rapidly and accurately, an initial value that can show a form that is similar to the experimental load-stroke curve must be selected even if the absolute magnitude of the load-stroke curve is different. Figs. 9 and 10 show the stress-strain relationship of each material. These were calculated from the unknown coefficients that were determined by the inverse analysis.

Fig. 11 shows the result (Material A, T=950° C and V=0.8 mm/sec) obtained by minimizing the difference in the barreling shapes of the deformed specimen in order to predict the interfacial friction condition. Table 2 lists the friction factors determined according to the temperature and the compression velocity of each material.

5.2 Verification of determined flow stress and interfacial friction condition

In order to verify the presented methodology and the predicted flow stress, additional experiments using the same materials were conducted. Further, the experimental results were

Table 2. Interfacial friction factor determined by inverse analysis.

Material	Temperature (℃)	Determined friction factor (m_f)	
		V_1	V_2
A	900	0.5973	0.5698
	950	0.6172	0.5867
B	950	0.6128	0.6011
	1000	0.6134	0.6052

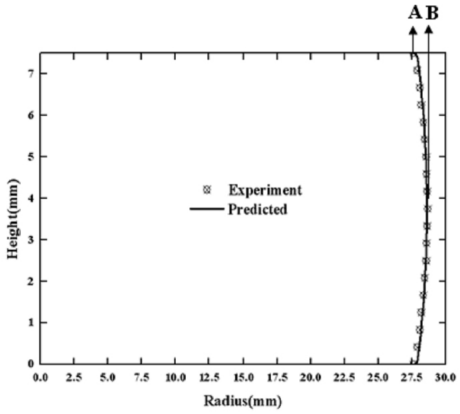

	Measured	Predicted
A	27.625 mm	27.629 mm
B	28.693 mm	28.621 mm

Fig. 11. Comparison of barreling shape between the measured and predicted shape of the ring at 50% compression for Material A; T=950℃ and V_2=0.8mm/sec.

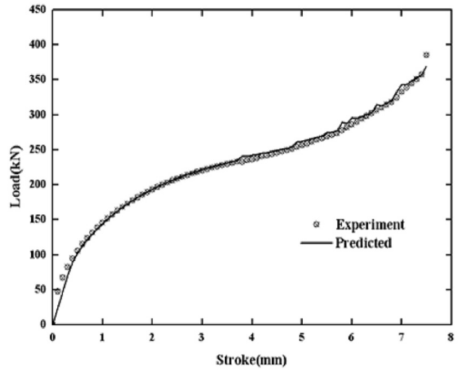

(a)

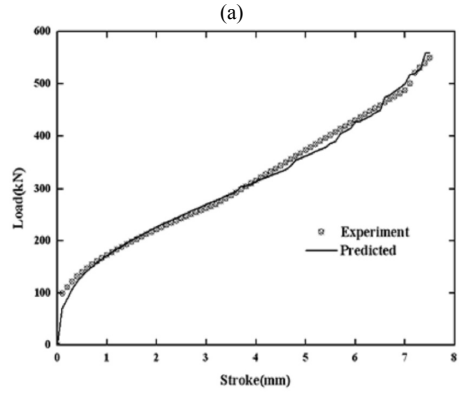

(b)

Fig. 12. Comparison of load-stroke curve between experimental and simulated results at V2=0.8mm/sec: (a) Material A, T=925℃ and (b) Material B, T=975℃.

Table 3. Process conditions of the experiment and the FE simulation.

Material	Temperature (℃)	Compression velocity (mm/sec)	Friction factor (m_f)	Material	Temperature (℃)	Compression velocity (mm/sec)	Friction factor (m_f)
A	925	0.8	0.5928	B	975	0.8	0.6082

Table 4. Process conditions of the experiment and FE simulation (cylinder specimen).

Material	Temperature (℃)	Compression velocity (mm/sec)	Friction factor (m_f)	Material	Temperature (℃)	Compression velocity (mm/sec)	Friction factor (m_f)
A	900	0.8	0.5836	B	950	0.8	0.6070
	925	0.8	0.5928		975	0.8	0.6082
	950	0.8	0.6020		1000	0.8	0.6093

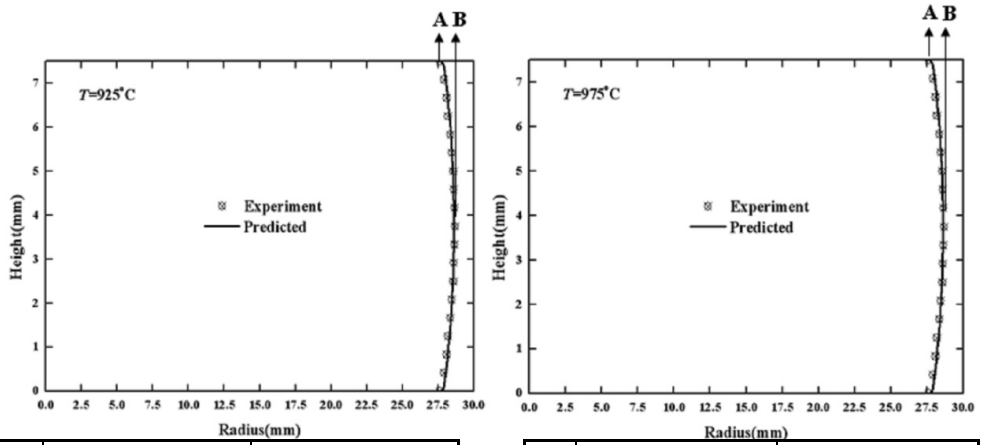

	Measured	Predicted
A	27.701 mm	27.699 mm
B	28.638 mm	28.629 mm

(a)

	Measured	Predicted
A	27.601 mm	27.706 mm
B	28.757 mm	28.768 mm

(b)

Fig. 13. Comparison of barreling shape between experimental and simulated results.

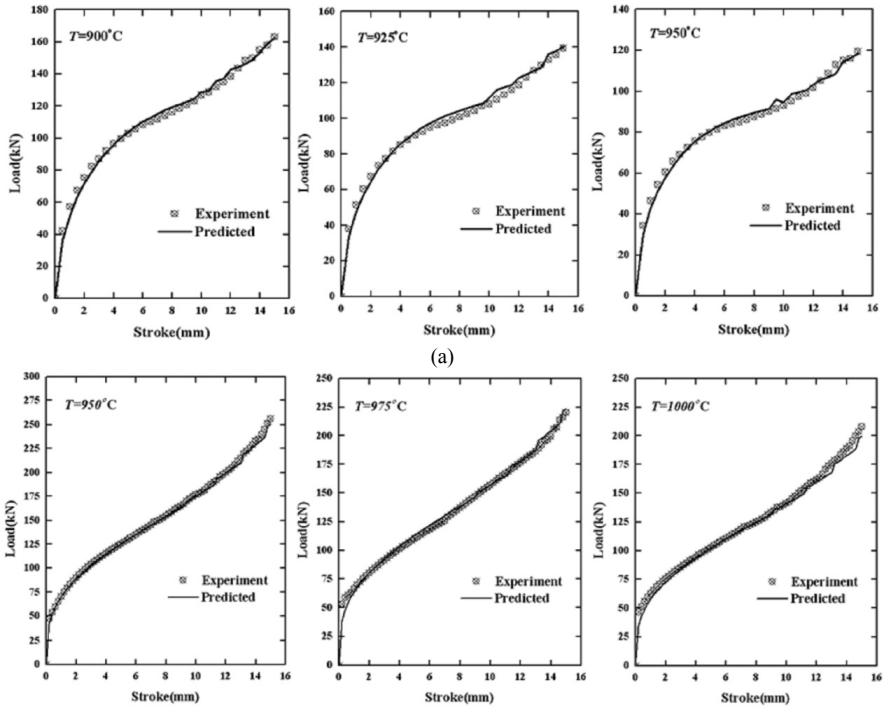

(a)

(b)

Fig. 14. Comparison of load-stroke curve between experimental and simulated results at V_2=0.8mm/sec: (a) Material A and (b) Material B.

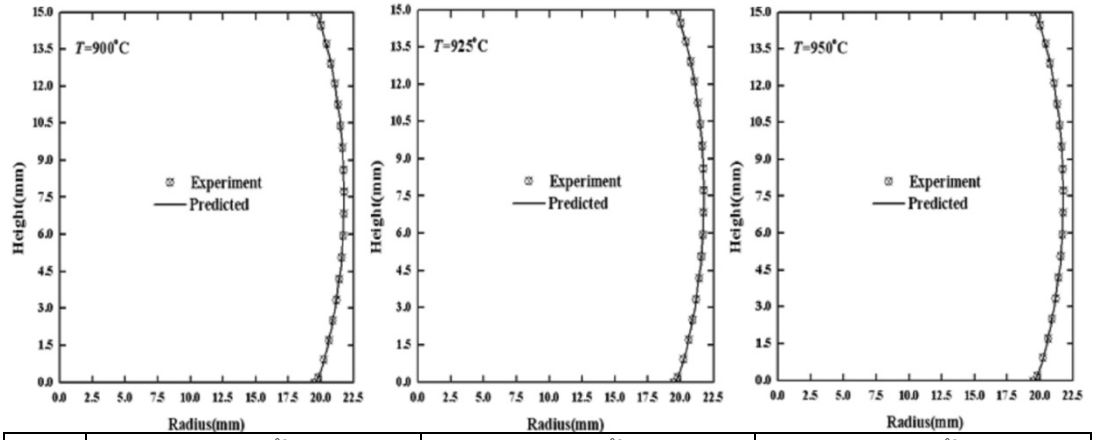

	T= 900℃		T= 925℃		T= 950℃	
	Measured	Predicted	Measured	Predicted	Measured	Predicted
A	19.281mm	19.701mm	19.262mm	19.640mm	19.235mm	19.565mm
B	21.771mm	21.790mm	21.782mm	21.806mm	21.794mm	21.813mm

Fig. 15. Comparison of barreling shape between measured and predicted barreling shape of the ring specimen at 50% compression for Material A: V_2=0.8mm/sec.

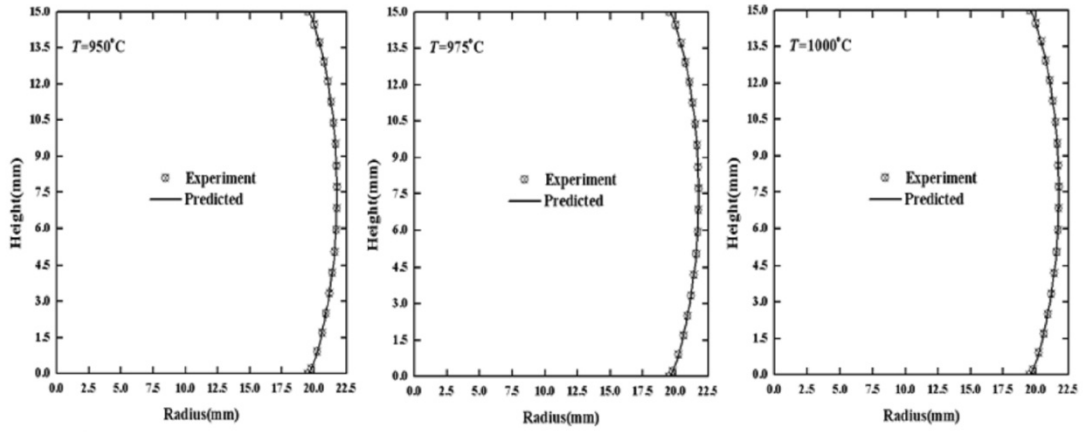

	T= 950℃		T= 975℃		T= 1000℃	
	Measured	Predicted	Measured	Predicted	Measured	Predicted
A	19.460mm	19.143mm	19.449mm	19.149mm	19.421mm	19.160mm
B	21.773mm	21.750mm	21.783mm	21.755mm	21.794mm	21.757mm

Fig. 16. Comparison of barreling shape between measured and predicted barreling shape of the cylinder specimen at 50% compression for Material A: V_2=0.8mm/sec.

compared with the FE simulation results to judge the validity of the flow stress and the interfacial friction condition obtained from Sec. 5.1..

First, ring compression tests were conducted under different temperature conditions. The process temperatures set for the middle values between the process temperatures of each material are listed in Table 1. The flow stress used in the FE simulation took advantage of a value to interpolate the flow stresses at two temperatures. Table 3 lists the process conditions for the ring compression tests. The difference in load-stroke data between the experimental and FE simulated results is defined as

$$\text{Difference}(\%) = \frac{1}{Ns}\sum_{j=1}^{Ns}\left\|\frac{F_{i.\exp.} - F_{i.sim}}{F_{i.\exp.}}\right\| \times 100\,, \tag{10}$$

where Ns is the number of sampling points, while $F_{i.exp.}$ and $F_{i.sim.}$ are the experimental and FE simulated results, respectively. Eq. (10) indicates whether the flow stresses and the interfacial friction conditions obtained from the ring compression tests are valid by presenting the difference in loads in the same stroke. Fig. 12 shows the compression of the experimental and simulated load-stroke curves. The differences calculated by Eqs . (10) were 2.85 and 3.65, respectively. These can be attributed to two reasons. The first reason is the error gen-

erated during the experiment. Although the experimental conditions are set correctly, a small error is certain to exist. The second reason is the numerical error generated by interpolating the flow stress data. Therefore, the abundant flow stress data for various temperatures and velocity conditions were secured in order to obtain more accurate FE simulated results.

Fig. 13 shows the comparison of the barreling shape of the deformed specimen between the experimental and FE simulated results. It is concluded that the data obtained from the above ring compression tests are acceptable because the difference is small. In order to verify the above flow stress and interfacial friction condition, additional verifications were performed by conducting cylinder compression tests for the information obtained from the ring compression tests.

The purpose is to judge the adequacy of the flow stress and the interfacial friction condition predicted from one experiment. The overall process conditions, including the temperatures, compression velocities, and friction factor, are listed in Table 4. The flow stress and the interfacial friction condition drawn by the ring compression test were used. Figure 14 shows the comparison of the load-stroke curves between the experimental and FE simulated results of each material. In the case of Material A, the differences were 2.371, 2.849, and 2.581, respectively. These results are reasonable since the average value was 2.603. The difference at 925°C is larger than that at other temperatures because a numerical error occurred when using the flow stress data interpolated at 900 and 950°C. In the case of Material B, the differences were 3.144, 3.645, and 3.323, respectively. The average value was 3.371. This result is similar to that of Material A. Figs. 15 and 16 show the comparison of the results of the barreling shape of the deformed specimen between the experiments and FE simulations according to the temperature. The figures indicate that experimental results are similar to the FE simulated results. The flow stress and the interfacial friction condition determined from the ring compression tests are valid.

Although the materials were the same, the flow stress of the materials can be differentiated according to the type of processes. For example, if the flow stress drawn by the simple compression tests was applied to the FE simulation of processes, such as the cutting or tension, some errors of the results can be generated. However, as in conducting a FE simulation, an error of this kind is generated inevitably. Therefore, in order to reduce the error that causes the inaccuracy of the FE simulated results, the abundant flow stress data should be secured according to various temperatures and velocity conditions.

6. Conclusions

In this study, the flow stress of some materials and the interfacial friction condition were predicted by using the ring compression test and inverse analysis. It was verified that the predicted flow stress and interfacial friction condition are reasonable by applying them to cylinder compression tests. The following conclusions were drawn from this study:

It is difficult to describe the deformation behavior because metal forming processes in hot working conditions are accompanied by phenomena such as dynamic recrystallization and recovery. In this study, the reliability of the flow stress function was verified by applying the information obtained from the ring compression test to the cylinder compression test. Therefore, it was concluded that the flow stress function suitably describes the deformation behavior of materials.

Inverse analysis is used to determine the flow stress and the interfacial friction condition. Its advantages are the determination of the flow stress and interfacial friction condition from one set of experiments, and thus it is simple and fast. In addition, it was verified that if the object function and the flow stress function are appropriate in the mathematical and physical aspects, results of the inverse analysis are quite reasonable without considering the microstructural data of materials.

Based on the result of the flow stress function used in the study being suitable for describing the deformation behavior of materials in hot working conditions, research about materials without the suitable flow stress data, such as high strength aluminum, magnesium alloys, and glass, will be required in the future.

References

[1] Y. Choi, H. K Kim, H. Y Cho, B. M Kim and J. C Choi, A method of determining flow stress and friction factor using an inverse analysis in ring compression test, *Journal of KSTP*, 22 (1998) 483-492.

[2] T. Altan, G. Ngaile and G. Shen, Cold and hot forging fundamentals and application, *ASM. International*, (2005) 25-49, 67-89.

[3] T. Altan, Material properties and cold forging lubricants, *Prepared for 2nd Cold and Warm precision Forging Workshop*, (2004).

[4] T. Altan and H. J. Cho, Simultaneous determination of flow stress and interface friction by finite element based inverse analysis, *Prepared for 53rd CIRP General Assembly*, (2003).

[5] T. Altan and H. J. Cho, Determination of flow stress and interface friction at elevated temperature by inverse analysis technique, 2003, *J. Mater. Process.Technol., 170* (2003) 64-70.

[6] R. Ebrahimi and A. Najafizadeh, A new method for evaluation of friction in bulk metal forming, *J. Mater. Process. Technol., 152* (2004) 136-143.

[7] S. Y. Lin and F. C. Lin, Prediction of fold defect in barreling formation of cylinder upsetting, *Finite Element in Analysis and Design*, 39 (2003) 325-341.

[8] S. Y. Lin and F. C. Lin, Influence of the geometrical conditions of die and workpiece on the barreling formation during forging-extrusion process, *J. Mater. Process. Technol.*, 140 (2003) 54-58.

[9] K. M. Kulkarni and S. Kalpakjian, A study of barreling as an example of free deformation in plastic working, *Journal of*

Engineering for Industry., 104 (1982) 79-83.
[10] J. A. Schey, T. R. Venner and S. L. Takomana, Shape changes in the upsetting of slender cylinders, *Journal of Engineering for Industry*, 104 (1982) 79-83.
[11] J. K. Banerjee, Barreling of solid cylinders under axial compression, *Transaction of the ASME.*, 107 (1985) 138-144.
[12] F. K. Chen and C. J. Chen, On the nonuniform deformation of the cylinder compression test, *Transaction of the ASME.*, 122 (2000) 192-197.
[13] R. Narayanasamy, R. S. N. Murthy, K. Viswabatham and G. R. Chary, Prediction of the barreling of solid cylinders under uniaxial compressive load, *Journal of Mechanical Working Technology.*, 16 (1988) 21-30.
[14] R. Narayanasamy, K. S. Pandey, Phenomenon of barreling in aluminium solid cylinders during cold upset forming, *J. Mater. Process. Thecnol.*, 70 (1997) 17-21.
[15] R. Narayanasamy, S. Sathiyanatayanan and R. Ponalagusamy, A study on barreling in magnesium alloy solid cylinders during cold upset forming, *J. Mater. Process. Technol.*, 101 (2000) 64-69.
[16] S. Malayappan and R. Narayanasamy, An experimental analysis of upset forming of aluminium cylindrical billets considering the dissimilar frictional conditions at flat die surfaces, *Int. J. Adv. Manuf. Technol.*, 23 (2004) 636-643.
[17] N. Kim and H. Choi, The prediction of deformation behavior and interfacial friction under hot working conditions using inverse analysis, *J. Mater. Process. Technol.*, (2007) be under examination.
[18] C. M. Sellars, The kinetics of softening processes during hot working of austenite, *Czech J. Phys. B35* (1984) 57-70.
[19] Y. Estrin and H. Mecking, An unified phenomenological description of work hardening and creep based on one- parameter models*, Acta Metall.* 32 (1984) 57-70.
[20] R. Colas, High temperature deformation of low carbon steels, *Mater. Forum* (1990) 14-253.
[21] K. P. Rao and E. B. Hewbolt, Development of constitutive relationships using compression testing of a medium carbon steel, ASME, *Journal of engineering materials technology*, (1992) 114-116.
[22] B. Kowalsksi, C. M. Sellars and M. Pietrzyk, Development of a computer code for the interpretation of results of hot plane strain compression tests, *ISIJ Int.* 40 (2000) 1230-1236.
[23] J. G. Lenard, M. Pietrzyk and L. Cser, Mathematical and physical simulation of the properties of hot rolled products, *Elsevier*, Amsterdam, (1999).
[24] D. Szeliga, J. Gawad and M. Pietrzyk, Inverse analysis for identification of rheological and friction models in metal forming, *J. Comput. Methods Appl. Mech. Eng.*, 195 (2006) 6778-6798
[25] J. S. Arora, *Introdution to optimum design*, Elsevier Academic Press, (2005).
[26] R. C. Gomzalez, R. E. Woods and S. L. Eddins, *Digital image processing using MATLAB*, Prentice Hall, (2004).

Mr. Kyoungmin Shin received his B.S. and M.S. degree from the department of Mechanical Engineering, Sogang University, Seoul, S. Korea in 2006 and 2009, respectively. Mr. Seo is currently working for Hyundai Engineering. His research interests are in the area of optimum design of electric motors, metal forming, and process design.

Naksoo Kim received his B.S. and M.S. degree from the department of Mechanical Design, Seoul National University in 1982 and 1984, respectively. He then went on to receive his Ph. D. degree from U.C. Berkeley. Dr. Kim had worked for the ERC/NSM at the Ohio State University as a senior researcher and Hongik University as an assistant professor. He is currently a professor at the department of mechanical engineering, Sogang University. Dr. Kim's research interests are in the area of metal forming plasticity, computer aided process analysis, and optimal design